AD-A111 438 SAN DIEGO STATE UNIV CA DEPT OF AEROSPACE ENGINEERIN--ETC F/G 20/4
UNSTEADY SYMMETRY-PLANE BOUNDARY LAYER AND 3-D UNSTEADY SEPARAT--ETC(U)
JAN 82 K C WANG, Z G FAN N00014-80-C-0307
UNCLASSIFIED AE/EM-TR-82-01 NL

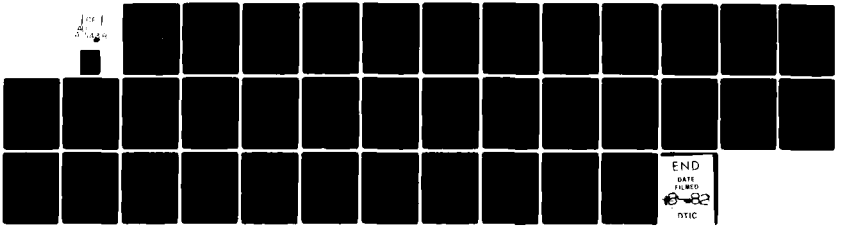

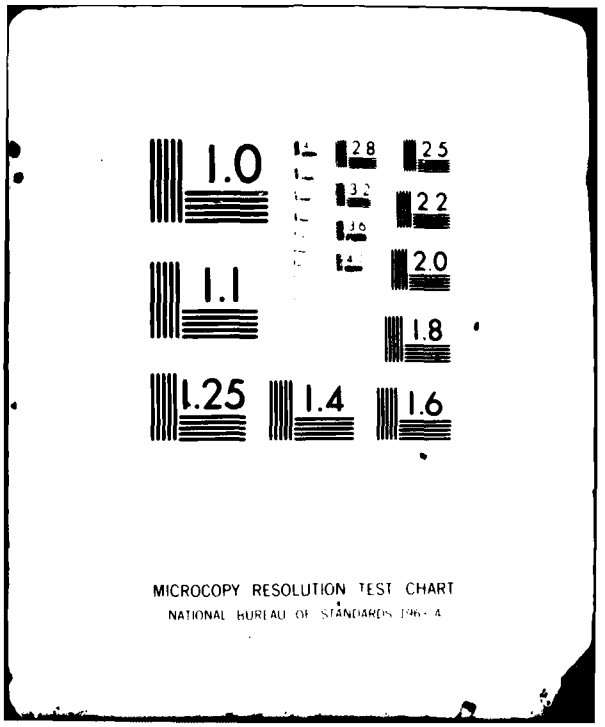
1.0
1.1
1.25
1.4
1.6
2.0
1.8
2.2
2.5
MICROCOPY RESOLUTION TEST CHART
NATIONAL BUREAU OF STANDARDS 1963-A

AE&EM TR-82-01

UNSTEADY SYMMETRY-PLANE BOUNDARY LAYER AND 3-D UNSTEADY SEPARATION, PART I. HIGH INCIDENCE

K. C. Wang and Z. Q. Fan

January 1982

Research Sponsored by Office of Naval Research under Contract N00014-80-C-0307

Approved for Public Release — Distribution Unlimited

SAN DIEGO STATE UNIVERSITY
College of Engineering
Department of Aerospace Engineering
and Engineering Mechanics
San Diego, CA 92182-0183
(714)265-6074

SECURITY CLASSIFICATION OF THIS PAGE (When Data Entered)

REPORT DOCUMENTATION PAGE		READ INSTRUCTIONS BEFORE COMPLETING FORM
1. REPORT NUMBER AE & EM-TR-82-01	2. GOVT ACCESSION NO. AD-A111 438	3. RECIPIENT'S CATALOG NUMBER
4. TITLE (and Subtitle) Unsteady Symmetry-Plane Boundary Layer and 3-D Unsteady Separation, Part I. High Incidence		5. TYPE OF REPORT & PERIOD COVERED Technical Report 6. PERFORMING ORG. REPORT NUMBER AE & EM TR-82-01
7. AUTHOR(s) K. C. Wang and Z. O. Fan		8. CONTRACT OR GRANT NUMBER(s) N00014-80-C-0307
9. PERFORMING ORGANIZATION NAME AND ADDRESS San Diego State University San Diego, CA 92182-0183		10. PROGRAM ELEMENT, PROJECT, TASK AREA & WORK UNIT NUMBERS NR 061-252
11. CONTROLLING OFFICE NAME AND ADDRESS Office of Naval Research 800 N. Quincy Street Arlington, VA 22217		12. REPORT DATE January 1982 13. NUMBER OF PAGES 32
14. MONITORING AGENCY NAME & ADDRESS(if different from Controlling Office)		15. SECURITY CLASS. (of this report) Unclassified 15a. DECLASSIFICATION/DOWNGRADING SCHEDULE

16. DISTRIBUTION STATEMENT (of this Report)

Approved for public release; distribution unlimited.

17. DISTRIBUTION STATEMENT (of the abstract entered in Block 20, if different from Report)

18. SUPPLEMENTARY NOTES

None

19. KEY WORDS (Continue on reverse side if necessary and identify by block number)

Unsteady boundary layer, numerical solutions
Unsteady separation
Three-dimensional flow

20. ABSTRACT (Continue on reverse side if necessary and identify by block number)

The symmetry-plane laminar boundary layer of an impulsively-started ellipsoid of revolution at high incidence is solved to shed light on some basic characteristics of three dimensional, unsteady flows. The governing equations are formally similar to those for the ~~three~~ 3-dimensional,

DD FORM 1 JAN 73 1473 EDITION OF 1 NOV 65 IS OBSOLETE
S/N 0102-LF-014-6601

Unclassified
SECURITY CLASSIFICATION OF THIS PAGE (When Data Entered)

steady case, so the same method of solution and computer programs previously developed were employed in the present work. The most important result obtained is concerned with the meridional skin friction $c^*_{f\mu}$. The zero-$c^*_{f\mu}$ point (at which $c^*_{f\mu}$ vanishes) does not, as expected, move forward as time increases, instead it remains over the rear body. As $t \to \infty$, it jumps to the front nose. This implies that there is no flow separation over the symmetry-plane at finite times. In the meanwhile, it is argued that separation must occur on two sides of the body. This situation leads us to propose a new unsteady separation sequence, i.e. an open type separation prevails at earlier times, while a closed type of separation occurs only at the steady-state condition. This sequence presents a sharp contrast to the conventional notion of unsteady separation which consistsof a series of closed separations only. Furthermore, this sequence with the time as the parameter is found to be similar to that for previously-studied steady flows with varying incidences.

t approaches infinity

$C(F_w)^*$

CONTENTS

ABSTRACT

The symmetry-plane laminar boundary layer of an impulsively-started ellipsoid of revolution at high incidence is solved to shed light on some basic characteristics of three dimensional, unsteady flows. The governing equations are formally similar to those for the three-dimensional, steady case, so the same method of solution and computer programs previously developed were employed in the present work. The most important result obtained is concerned with the meridional skin friction $c_{f\mu}$. The zero-$c_{f\mu}$ point (at which $c_{f\mu}$ vanishes) does not, as expected, move forward as time increases, instead it remains over the rear body. As $t \to \infty$, it jumps to the front nose. This implies that there is no flow separation over the symmetry-plane at finite times. In the meanwhile, it is argued that separation must occur on two sides of the body. This situation leads us to propose a new unsteady separation sequence, i.e. an open type separation prevails at earlier times, while a closed type of separation occurs only at the steady-state condition. This sequence presents a sharp contrast to the conventional notion of unsteady separation which consists of a series of closed separations only. Furthermore, this sequence with the time as the parameter is found to be similar to that for previously-studied steady flows with varying incidences.

1. INTRODUCTION

The complexity of boundary layer research increases from two-dimensional steady problems to two-dimensional unsteady, three-dimensional steady and finally to three-dimensional unsteady problems. Considerable progress has been made in recent years to two-dimensional unsteady and three dimensional steady problems, but the three-dimensional, unsteady area remains to be the last frontier to be fully exploited. Three-dimensional, unsteady solutions are very scarce. A classical work in this subject is due to Squire (1954) who, using a time-series expansion method investigated the motion of an impulsively-started ellipsoid. Recent publications in this area include, for example, those of Dwyer and Sherman (1979) and Williams (1980).

As a prelude to full three-dimensional investigations, the present work considers the symmetry-plane boundary layer over an ellipsoid of revolution. The steady counterpart of this problem was studied before by one of the present authors (Wang 1970) and later by Cebei et al (1980). Although consideration was restricted to the symmetry-plane, the results revealed features of fundamental significance for (steady) three-dimensional flows in general (Wang 1974a, 1976). It was our original motivation that the present work will achieve the same for the corresponding unsteady case. Our results to be presented later seem to bear out this expectation.

The specific unsteady motion considered is that of an impulsive start. This problem provides an interesting contrast to the classical impulsively-started circular cylinder problem. In the latter case, the zero-skin-friction point starts from the rear stagnation point, moves gradually forward as time increases and approaches finally the steady-state separation position ($\theta \cong 104.5°$). For the present ellipsoid case, the zero-skin-friction point on the leeside symmetry-plane was at first thought to move very much the same way. From our previous investigations (Wang 1974b), the steady-state position of the zero-skin-friction point on

the symmetry-plane is located at the front nose, while a closed type of separation prevails over the whole body (figure 1c). Consequently if the zero-skin-friction point on the leeside symmetry-plane gradually moves forward as expected, then it seems natural to think that similar overall separation pattern would also prevail over the body at earlier times as well. This leads to an unsteady sequence of developments as depicted in figures 1(a)-(c), each figure displays a closed type of separation except the separated area expands with time. This sequence represents, in fact, the conventional idea of unsteady separation. However, in Section 4, we shall show that our present results did not turn out the way as expected and in Section 5, we shall propose instead a new sequence of unsteady separation consisting of both open and closed types of separation patterns.

Finally we would like to comment on the current status of the boundary layer theory relative to the "thin layer" theory (Pulliam and Steger 1980, Hsieh 1981). The basic idea of the "thin layer" approximation is similar to that of the boundary layer theory except the pressure is not imposed according to an inviscid solution, instead it is calculated along with the boundary layer. This allows the inviscid boundary layer interaction and hence broadens the range of validity beyond that of the boundary layer theory. However a thin-layer problem is mathmatically an elliptical problem in the space coordinates, whereas a boundary layer problem is parabolic. Solving an elliptical problem requires larger computer storage and longer computation time so that adequate resolutions were found not possible on a CDC 7600 computer.

This difficulty led later to the idea of parabolicization, i.e. treating an elliptic problem in a parabolic fashion (Schiff and Steger 1980). This procedure requires that there is no upstream pressure influence in the main flow direction. The latter condition is best satisfied in a supersonic cone flow for which the longitudinal (or meridional) perssure gradient is identically zero.

However even in this particular case, the above condition is not completely met because the flow is no longer strictly conical when the inviscid-boundary layer interaction is considered. In a general supersonic flow, there is always a subsonic part of the boundary layer where the above condition cannot be satisfied. For subsonic flows, paraboliciz ation cannot be justified. Thus thin-layer theory is more general, but is accompanied by the above shortcomings. At the present state of the art, it appears that boundary layer theory is still the most appropriate approach for general three-dimensional viscous flows, because even to this lower approximation (compared to the thin-layer version), unsteady solutions are still not available. On the other hand, one may favor the thin-layer version when computer's storage and time are not of much concern under certain circumstances, because it avoids to solve the inviscid and viscous flows separately aside from the interaction between them mentioned above.

2. EQUATIONS

The governing equation for the present symmetry-plane boundary layer written in non-dimensional form consists of

$$\frac{\partial u}{\partial t} + u\frac{\partial u}{h_\mu \partial \mu} + w\frac{\partial u}{\partial z} = \frac{-\partial p}{h_\mu \partial \mu} + \frac{\partial^2 u}{\partial z^2}\ , \tag{1a}$$

$$\frac{\partial v_\theta}{\partial t} + u\frac{\partial v_\theta}{h_\mu \partial \mu} + w\frac{\partial v_\theta}{\partial z} + \frac{v_\theta^2}{r} + \frac{uv_\theta}{r}\frac{\partial r}{h_\mu \partial \mu} = -\frac{\partial^2 p}{r\partial \theta^2} + \frac{\partial^2 v_\theta}{\partial z^2}\ , \tag{1b}$$

$$\frac{\partial u}{h_\mu \partial \mu} + u\frac{\partial r}{r h_\mu \partial \mu} + \frac{v_\theta}{r} + \frac{\partial w}{\partial z} = 0. \tag{1c}$$

Aside from the unsteady terms, these equations are otherwise identical to these for the steady case treated before (Wang, 1970). The same notations are also used. Briefly, referring to figure 2, α is the incidence angle, μ and θ are two surface coordinates, z is the normal coordinate. u, v and w are the corresponding velocities, U and V are the inviscid velocities at the outer edge. h_μ and r are the metric coefficients and r, in fact, is also the cross-sectional radius.

$$h_\mu = \left[(1 - e^2\mu^2) / (1 - \mu^2)\right]^{\frac{1}{2}},$$

$$r = \left[(1 - e^2)(1 - \mu^2)\right]^{\frac{1}{2}}$$

where

$$e = (1 - b^2/a^2)^{\frac{1}{2}}\ .$$

a and b are the semi-major and -minor axis of the ellipsoid.

At the plane of symmetry, $v \equiv 0$, so that $v_\theta (= \partial v/\partial\theta)$ is taken as an independent variable along with u and w. The boundary conditions are

$$u = U,\ v_\theta = V_\theta (\text{i.e. } \partial V/\partial\theta) \quad \text{at } z \to \infty\ ,$$

$$u = v_\theta = 0 \quad \text{at } z = 0, \tag{2a,b,c}$$

where U, V_θ and the pressure gradients are known;

$$U = \frac{1}{(1-e^2\mu^2)^{\frac{1}{2}}}\left[(1+k_a)(\cos\alpha)(1-\mu^2)^{\frac{1}{2}} + (b/a)(1+k_c)(\sin\alpha)\,\mu\cos\theta\right],$$

$$V_\theta = (1+k_c)\sin\alpha\cos\theta, \qquad (3a,b,c,d)$$

$$-\frac{\partial p}{h_\mu \partial\mu} = \frac{(1+k_a)^2\cos^2\alpha}{(1-e^2\mu^2)^{3/2}}\left[(1-\mu^2)^{\frac{1}{2}}+\lambda\mu\cos\theta\right]\left\{-\mu+\lambda(\cos\theta)(1-\mu^2)^{\frac{1}{2}} + \frac{e^2\mu}{1-e^2\mu^2}\left[1-\mu^2+\lambda\mu\cos\theta(1-\mu^2)^{\frac{1}{2}}\right]\right\}$$

$$-\frac{\partial^2 p}{\partial\theta^2} = \frac{1}{(b/a)}(1+k_a)(1+k_c)\cos\alpha\,\sin\alpha\left\{\lambda-\left(\frac{b}{a}\right)^2\frac{\mu\cos\theta}{1-e^2\mu^2}\left[(1-\mu^2)^{\frac{1}{2}}+\lambda\mu\cos\theta\right]\right\}$$

with

$$\lambda = \left(\frac{b}{a}\right)\frac{(1+k_c)\sin\alpha}{(1+k_a)\cos\alpha}$$

$$k_a = \left[\frac{1}{2e}\log\frac{1+e}{1-e}-1\right]\Bigg/\left[\frac{1}{1-e^2}-\frac{1}{2e}\log\frac{1+e}{1-e}\right], \quad k_c = \frac{1}{1+2k_a}$$

Based on the u-velocity, the skin friction and the displacement thickness are defined by

$$c_{f\mu} = \frac{1}{\sqrt{R}}\left(\frac{\partial u}{\partial z}\right)_{z\to 0}, \qquad (4a,b)$$

$$\Delta^*_\mu = \int_0^\infty (1-u/U)\,dz .$$

Analogously, we define based on the v_θ - profile,

$$(c_f)_{v\theta} = \frac{1}{\sqrt{R}}\left(\frac{\partial v_\theta}{\partial z}\right)_{z\to 0}, \qquad (4c,d)$$

$$\Delta^*_{v\theta} = \int_0^\infty (1-v_\theta/V_\theta)\,dz .$$

Although the v_θ- profile has always been calculated in the symmetry-plane type of boundary layer studies, analogous displacement thickness $\Delta^*_{v\theta}$ was, however, not considered except by Wang (1971a). Even there $\Delta^*_{v\theta}$ was not recognized to be needed in evaluating the total displacement thickness.

Moore and Ostrach (1957) derived the equation for the unsteady total displacement thickness Δ^*,

$$\nabla \cdot \left[\rho_1 q_1 \Delta^* - \int_0^\infty (\rho_1 \vec{q}_1 - \rho \vec{q}) dz\right] + \frac{\partial}{\partial t}\left[\rho_1 \Delta^* - \int_0^\infty (\rho_1 - \rho) dz\right] = 0 \ . \qquad (5a)$$

In applying this equation to the symmetry-plane case, care must be taken to incorporate $\Delta^*_{v\theta}$ into the final expression;

$$\frac{\partial \Delta^*}{\partial t} + \frac{1}{r h_\mu} \frac{\partial}{\partial \mu}\left[rU(\Delta^* - \Delta^*_\mu)\right] + \frac{v_\theta}{r}(\Delta^* - \Delta^*_{v\theta}) = 0. \qquad (5b)$$

In the literature, only Δ^*_μ has been reported. Here we shall present results of both Δ^*_μ and $\Delta^*_{v\theta}$, but the calculation of Δ^* is still not carried out yet.

3. METHOD OF SOLUTION

The equations (1a,b,c) are similar in structure to those for three-dimensional, steady boundary layers investigated before (Wang 1974a). So the same numerical methods and computer programs developed earlier were used for the present work.

3.1. Initial Profiles.

To start the computation, two sets of initial profiles, temporal and spatial, are required.

Temporal Initial Profiles ($t=t_o$). Immediately after (impulsive) starting, potential flow prevails. For the temporal initial profiles, the usual first approximation of a small-time expansion is adequate, i.e.

$$u(t_o, \mu, z) = U(\mu) \operatorname{erf}\left(\frac{z}{2\sqrt{t_o}}\right), \tag{6a}$$

$$v_\theta(t_o, \mu, z) = V_\theta \operatorname{erf}\left(\frac{z}{2\sqrt{t_o}}\right), \tag{6b}$$

where erf is the error function.

Spatial Initial Profiles ($\mu=\mu_o$). Based on the argument that diffusion and convection affect the downstream flow only, so that solutions near the stagnation point are nearly independent of time. Thus the required spatial initial profiles may be provided by the steady symmetry-plane solutions near the stagnation point.

3.2. Dependence Zone

For steady three-dimensional boundary layers, calculation was found to have to follow the zone of dependence rule (Raetz 1957, Wang 1971b). For steady, symmetry-plane problems, the wedge-shaped dependence zone shrinks to the symmetry-plane itself and it was found (Wang 1970) that calculation stops at the onset of the reversal of the u-velocity profile, but reversal of the v_θ-profile was unexpectedly calculated with no sign of any difficulty. This result was at first looked upon with suspicion, but later calculation of the full three-dimension problems as well as the repeat

calculation of the same symmetry-plane problem confirmed that result to be correct. However, a theoretical explanation was not available.

For unsteady cases, two-dimensional or the symmetry-plane, an analogous zone of dependence (Wang 1975, 1979) must be observed. So at the beginning of the present work, we were faced again with the same question; what are precisely the differences in logic for the calculation of the u-profile and the v_θ-profile? In the unsteady case, we, in fact, further know that reversal of u-profile can be calculated up to separation unlike in the steady case where calculation of the reversal of the u-profile is prohibited (Wang 1979).

To provide the missing explanation, we carried out a characteristics study of the system of equations (1a,b,c). The determinants (Wang 1971b) of the characteristics and subcharacteristics were found respectively to be

$$Q = -\nu^2 \left(\frac{\partial \Omega}{\partial z}\right)^5 , \tag{7a}$$

$$Q \quad \frac{\partial \Omega}{\partial z}\left(\frac{\partial \Omega}{\partial t} + \frac{u}{h_\mu}\frac{\partial \Omega}{\partial \mu} + w\frac{\partial \Omega}{\partial z}\right)^2 , \tag{7b}$$

which shows that the addition of equation (1b) for v_θ (compared to equations for two-dimensional cases) merely increase the power from 3 (Wang 1975) to 5 in equation (7a) and from 1 to 2 in equation (7b). Otherwise the same dependence rule applies to both the two-dimensional and the symmetry-plane problems. The underlying reason why reversal of v_θ is not prohibited by the dependence rule is recognized due to the fact that in both equations (1a,b), the differential operator

$$\frac{\partial}{\partial t} + u\frac{\partial}{h_\mu \partial \mu} + w\frac{\partial}{\partial z}$$

does not involve v_θ. Yet it is this operator which determines the subcharacteristics in equation (7b).

3.3. Computational Details

The initial time t_o was set to be 0.01 and the initial space μ_o was taken

to be -0.984, very close to the front vertex ($\mu = -1.0$). With initial profiles, calculation marches from the front stagnation point toward the rear body at a fixed time t. At each station (μ,t), solution between the body ($z=0$) and the outer edge ($z \to \infty$) is implicitly calculated. Then the same process is repeated as time increases from t to $t+\Delta t$ until the whole problem is completed.

At high incidence (45°), large pressure gradients prevail in both the meridional and circumferential directions, especially over the two ends. Computational difficulties due to poor convergence were experienced at the beginning of the present work, it was only diagnosed later that unusually small steps must be employed. Figure 3 compares the results of two calculations with different mesh sizes. Although $\Delta t = \Delta\mu = 0.005$ is normally considered to be small, results still show large deviations.

Immediately after the impulsive start ($t<0.05$), relatively large meshes ($\Delta t = 0.005, \Delta\mu = 0.005$) could be used. Then smaller space step ($\Delta\mu = 0.00125$ was required near two ends of the body, finally Δt must also be reduced (0.0025 and 0.00125). For $0.05 \leq t \leq 0.16$, our computation covers the whole leeside symmetry-plane; $\Delta t = 0.00125$, but two different $\Delta\mu$'s were used to save the computing time. These values are 0.00125 for two ends, and 0.005 for the mid-body. For $0.16 \leq t \leq 1.0$, only the front nose portion was calculated (reason is given in section 4), $\Delta t = 0.00125$, $\Delta\mu = 0.00125$ and even 0.000625. Such three-dimensional (t, μ, z) computations with small steps are very expensive. Compared to that for the u-profile, calculation of the v_θ-profile especially demands finer steps in order to satisfy the outer-edge condition (i.e. to merge smoothly with V_θ). This is attributed to the lateral (circumferential) pressure gradient being more severe than the meridional pressure gradient for the problem under consideration.

4. RESULTS OF HIGH INCIDENCE

The windside symmetry-plane problem is more straightforward, so only the leeside results ($\alpha = 45°$) are presented in details. For low to moderate incidences, the unsteady growth is expected to have a very different structure, and will be reported separately later on.

4.1 Pressure Variation

Figure 4 gives the variation of pressure p, longitudinal pressure gradient $\partial p/h_\mu \partial\mu$ and lateral pressure curvature $\partial^2 p/r\partial^2\theta$. The last two are directly involved in equations (1b,c). The pressure gradient is fairly mild over the mid-body, but extremely large near two ends. This suggests that computational difficulties as well as the most interesting features of fluid mechanics would likely occur near the ends also.

4.2 Skin Friction $c_{f\mu}$

Figure 5(a) gives the meridional skin-friction, $c_{f\mu}$, along the leeside symmetry-plane. At first, $c_{f\mu}$ decreases from the front to become zero at the rear stagnation point. But as time increases, two important features emerge: (1) The zero-$c_{f\mu}$ point does not gradually move forward, instead it remains over the rear body; (2) there develops a minimum point at the front, and furthermore, this minimum-$c_{f\mu}$ continues to decrease until finally it becomes zero. At that time, the zero-$c_{f\mu}$ point suddenly jumps from the rear to the front.

Calculations over the entire leeside symmetry-plane were carried out up to $t = 0.16$. At that stage, it was felt that the abovementioned two features were established, and the remaining task was only to determine how fast this minimum-$c_{f\mu}$ will approach zero. For this purpose, it is unnecessary to calculate over the entire symmetry-plane. Hence later calculations were limited to the front body only in order to save the computing cost. The details of $c_{f\mu}$ from the later

calculations are shown in figure 5(b). As time increases, it is seen that $c_{f\mu}$ approaches zero at an extremely slow rate. For example, between t = 0.5 and 1.0, $(c_{f\mu})_{min}$ is only reduced from 0.2403 to 0.1828. With $\Delta t = 0.0025$, this part of the calculation alone took 200 cycles with $\Delta\mu = 0.000625$. The slow change led us to interpret that $(c_{f\mu})_{min.}$ approaches zero asymptotically as $t \to \infty$.

4.3. Analogous Skin Friction $(c_f)_{v\theta}$

Figures 6(a)-(b) give the corresponding results of the analogous skin friction $(c_f)_{v\theta}$ based on the profile of v_θ. $(c_f)_{v\theta}$ determines among others the sign of v-velocity near but off the symmetry-plane. Change of the sign of $(c_f)_{v\theta}$ means the reversal of the v-velocity. At small times ($t \leq 0.10$), figure 6(a) shows the point of zero-$(c_f)_{v\theta}$, R_1, moving gradually forward from the rear stagnation point. At $0.10 \leq t \leq 0.13$, additional v-reversals occur at R_2 and R_3 over the front. As time further increases, R_2 moves rearward and merges with R_1, then disappearing altogether. At $t > 0.13$, there exists only R_3 at the front. The above description of the zero-$(c_f)_{v\theta}$ point is summarized in figure 6(c) which displays clearly its non-monotonic behavior. At $0.10 \leq t \leq 0.13$, there are R_1, R_2 and R_3 (corresponding to t= 0.12). As time increases, R_1 moves from D (i.e. rear stagnation point) to C, R_2 from B to C and R_3 from B toward A. The curve ABCD divides the μ,t-plane into two parts; i.e. whether v-velocity near the symmetry-plane is reversed or not.

The surface flow pattern near the symmetry-plane in accordance with figure 5 and 6 are illustrated in figure 7. In figure 7(a), the flow at earlier times points back and up (except between R_1 and A_R where A_R stands for the rear stagnation point), whereas in figure 7(d), the flow points back and down. Figures 7(b)-(c) indicate the intermediate changes. Figure 7(e) suggests that after the point of zero-$c_{f\mu}$ jumps to the front, the steady-state separation point S_s ($\mu = -0.921$) is located downstream of R_3 ($\mu = -0.955$). This makes S_s as a saddle point of separation as expected. More about separation will be discussed

in section 5. In any case, the changes of v-velocity's sign back and forth is rather unusual, indicating the complex structure involved in an unsteady development.

4.4 Basic Profiles

The reasons about why $c_{f\mu}$ and $(c_f)_{v\theta}$ show unusual variations can all be traced out from the results of the corresponding basic profiles. Figure 8(a) shows the u-velocity profiles at t = 0.12. The non-monotonic variation of $c_{f\mu}$ shown in figure 5(a) is a reflection of the intersection of the profiles at different μ-stations. Near the body ($z<0.4$), the curve for $\mu = 0.716$ stands between those for $\mu = -0.946$ and -0.133. This implies that $c_{f\mu}$ is the smallest at the front body $\mu = -0.946$, increases at the mid-body $\mu = -0.133$ and decreases at the rear body $\mu = 0.716$. Figure 8(b) shows the profile of v_θ at t = 0.12. That the curve for $\mu = -0.133$ falls between those for $\mu = -0.946$ and -0.833 (rather than between $\mu = -0.833$ and 0.716) is again responsible for the sign of v-velocity to change back and forth.

4.5 Displacement Thickness

Figure 9 shows the displacement thicknesses Δ^*_μ and $\Delta^*_{v\theta}$. Unlike in the normal situation, these thicknesses do not grow montonically in the downstream direction, instead they increase sharply near the front nose and then curve downward immediately thereafter. This phenomenon again follows from the profiles shown in Figures 8(a)-(b), and was similarly noted before in the steady cases (Wang 1970, 1971a). $\Delta^*_{v\theta}$ increases much faster than Δ^*_μ with increasing time, reflecting the dominance if the circumferential flow. $\Delta^*_{v\theta}$ is, in fact, presented here for the first time, its importance has been to date overlooked in the literature.

5. IMPLICATION OF 3-D UNSTEADY SEPARATION

The variation of the meridional skin-friction $c_{f\mu}$ discussed in connection with figure 5(a) has an important bearing with respect to three-dimensional separation, i.e. separation on the whole body rather than along the symmetry-plane itself. A similar situation was noted previously in the steady case (Wang 1971a) from which figure 10 is reproduced to show the corresponding skin friction $c_{f\mu}$. As the incidence increases, there develops a minimum point of $c_{f\mu}$ over the front nose. This minimum dips deeper until it becomes zero. When that happens, the zero-skin-friction point jumps from the rear body to the front nose. Comparing figures 10 and 5(a), it is clearly seen that in both cases, the zero-skin-friction point remains over the rear body, while a minimum develops over the front nose. The varying parameters are the time in figure 5(a) and the incidence in figure 10.

The behavior of $c_{f\mu}$ in figure 10 led us later to conceive the open vs closed separation concept (Wang 1972, 1974a, 1976). The basic idea of a closed separation fits well with the traditional notion of separation, but that of an open separation proves to be just the opposite. In the past few years, the open separation idea has been confirmed by many experiments and numerical solutions (Wang 1976, 1982). By the same reasoning, we propose here an unsteady counterpart of the open-vs-closed separation sequence. The arguments are as follows:

For the steady two-dimensional case or the steady symmetry-plane case (Wang 1970), separation is marked by the vanishing of the meridional skin friction $c_{f\mu}$. For the unsteady, two-dimensional case, it was demonstrated (Wang 1979) that separation is identified by the running-together of the analogous limiting streamlines in the μ, t-plane, the same idea holds for the unsteady, symmetry-plane problem concerned here. By this criterion, although the vanishing of $c_{f\mu}$ is not synonymous to separation, yet separation occurs only after $c_{f\mu}$ goes to zero and

then becomes negative. However, in section 4, since we noted already that the zero-$c_{f\mu}$ point does not continue to move forward, so we conclude that there is no flow separation on the leeside symmetry-plane. Furthermore, in order to have the separation patterns of figure 1b,c, there must be a zero-$c_{f\mu}$ point on the symmetry-plane. This condition is again denied by the present results, so we conclude that the sequence shown in figure 1(a)-(c) is not to happen.

We must next emphasize that lack of separation on the symmetry-plane does not mean there is no separation on the sides of the body. In fact, due to the fact that the circumferential flow over most of the body is subject to larger pressure gradient than the meridional flow, so that a mainly lateral separation must occur on two sides of the symmetry-plane at much earlier times. Besides, we knew beforehand that the steady-state separation at such a high incidence is of a closed type as shown in figures 1c or 11c. It is inconceivable that such a whole closed separation pattern is established instantaneously at the moment when the zero-$c_{f\mu}$ point jumps to the fore body. Based on these reasons, we propose that the likely sequence of developments is as depicted in figures 11a,b,c. In other words, an open type of separation starts first ($t=t_1$) over the rear body, extends forward as time increases ($t=t_2$) until the open separation line finally intercepts the symmetry-plane upon the jump of the zero-$c_{f\mu}$ point from the rear body to the front, thus completing the formation of a closed separation for the steady-state condition.

The proposed unsteady sequence of separation is analogous to a steady counterpart suggested by one of the present authors (Wang 1976). While the latter has been confirmed by experiments and calculations, we expect that experimental demonstration of the unsteady separation will be more difficult, whereas full three-dimensional unsteady boundary layer solutions also remain to be reported.

The preceding conclusion of no separation of finite times touches on an interesting story. Over the past few years, there was a controversy (Wang 1981) on this question in the literature. Cebeci (1979) advanced a similar idea in connection with an impulsively-started circular cylinder problem. His idea was disputed by other researchers (including one of the present authors, Wang) and has since been known to be in error for the cylinder case. But ironically, our present results do seem to provide an example in agreement with his idea as far as the separation on the symmetry-plane is concerned. The circumstances here are of course different from what he originally conceived, the symmetry-plane separation is only a part of the overall three-dimensional separation, whereas his problem was a two-dimensional one.

6. CONCLUSIONS

For an impulsively-started symmetry-plane problem at high incidence, the circumferential flow near the symmetry plane was found to reverse its direction back and forth.

The variation of the meridional skin friction $c_{f\mu}$ is surprisingly found to be similar to that for the corresponding steady case studied before, although the varying parameter is the time in the present unsteady case, while the same is the incidence angle in the previous steady case. The zero-$c_{f\mu}$ point was found to remain over the rear body at all finite times until it jumps to the front nose to reach the steady-state condition at $t \to \infty$.

Since the zero-c_{fu} point does not gradually move forward, it is concluded that there is no separation on the symmetry-plane at all finite times. Instead an open separation is likely to develop first over the sides of the rear body, and gradually extends forward. When the zero-$c_{f\mu}$ point jumps to the front nose and the open separation line intersects the symmetry-plane, then a closed separation is formed at the steady-state condition. On the one hand, this open and closed separation sequence provides a striking contrast to the conventional notion of unsteady sequence consisting of closed separations only. On the other hand, this sequence with time as the parameter is found to be similar to that for steady flows with varying incidences. Our open vs. closed separation idea originally conceived for steady flows is now extended to unsteady flows.

7. REFERENCES

Cebeci, T. (1979). The Laminar Boundary Layer on a Circular Cylinder Started Impulsively from Rest. Journal of Computational Physics, 31, 153-172.

Cebeci, R., Khattab, A. K. and Stewartson, K. (1980). On Nose Separation. J. Fluid Mech. 97, 435-454.

Dwyer, H., and Sherman, F. R. (1979). Some Characteristics of Unsteady Two- and Three-Dimensional Reversed Boundary Layer Flows. AIAA Paper 79-1518.

Hsieh, T. (1981). Calculation of Viscous Sonic Flow Over Hemisphere-Cylinder at 19° Incidence: Capturing of Nose Vortices. AIAA Paper 81-0189.

Moore, F. K. and Ostrach, S. (1957). Displacement Thickness of the Unsteady Boundary Layer. J. Aero. Sci. 24, 77-78.

Pulliam, T. H. and Steger, J. L. (1980). Implicit Finite-Difference Simulations of the Dimensional Compressible Flow. AIAA Journal, 18,2, 159-167.

Raetz, G. S. (1957). A Method of Calculating Three-Dimensional Laminar Boundary Layers of Steady Compressible Flows, Report NAI 58-73, Northrop Corporation.

Schiff, E. B. and Steger, J. L. (1980). Numerical Simulation of Steady Supersonic Viscous Flow. AIAA Journal. 18, 12, 1421-1430.

Squire, L. C. (1954). Boundary Layer Growth in Three Dimensions. Phil. Mag. 7, 45, 1272-83.

Wang, K. C. (1970). Three-Dimensional Boundary Layers Near the Plane of Symmetry of a Spheroid at Incidence. J. Fluid Mech., 43,187-209.

Wang, K. C. (1971a). Three-Dimensional Laminar Boundary Layer Over Body of Revolution at Incidence, Part V. Further Investigation Near the Plane of Symmetry. Martin Marietta Corp., RIAS TR-71-14c. Also AIAA Journal, 12, 7, 949-958, (1974).

Wang, K. C. (1971b). On the Determination of the Zones of Influence and Dependence for Three-Dimensional Boundary-Layer Equations. J. Fluid Mech. 48, 2, 397-404.

Wang, K. C. (1972). Separation Patterns of Boundary Layer Over An Inclined Body of Revolution. AIAA Journal, 10, 8, 1044-1050.

Wang, K. C. (1974a). Boundary Layer Over a Blunt Body at High Incidences with an Open-Type of Separation. Proc. Roy. Soc., London, A340,33-55.

Wang, K. C.(1974b). Boundary Layer Over a Blunt Body at Extremely High Incidences. The Physics of Fluids, 17, 7. 1381-1385.

Wang, K. C. (1975). Aspects of 'Multitime Initial Valued Problem' Originating from Boundary Layer Equations. Physics of Fluids, 18, 8, 951-955.

Wang, K. C. (1976). Separation of Three-Dimensional Flow. Proc. Lockheed Georgia Company Viscous Flow Symposium, LG 77ER0044, Atlanta, GA, 341-414. Also Martin Marietta Labs TR 76-54c.

Wang, K. C. (1979). Unsteady Boundary Layer Separation. Martin Marietta Labs. TR-79-16c.

Wang, K. C., (1981). On Current Controversy of Unsteady Separation. Proceeding of Symposium on Numerical and Physical Aspects of Aerodynamic Flows, Long Beach, CA.

Wang, K. C. (1982). New Development of Open Separation. Proceeding of IUTAM Symposium for Three-Dimensional Turbulent Boundary Layers, Berlin Germany, March 29 - April 1, 1982 (in preparation).

Williams, J. C. (1978). On the Nature of Unsteady Three-Dimensional Laminar Boundary-Layer Separation. J. Fluid Mech. 88, 241-258.

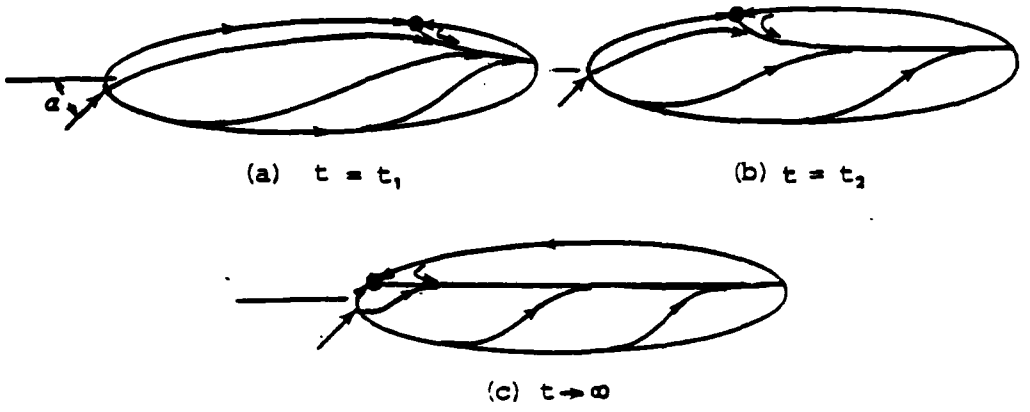

Figure 1. Conventional sequence of unsteady separation

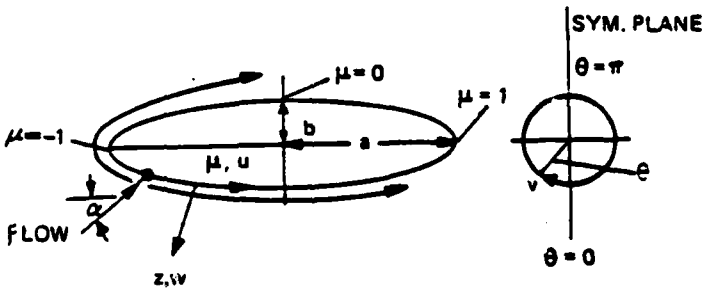

Figure 2. Ellipsoid of revolution, coordinates and notations

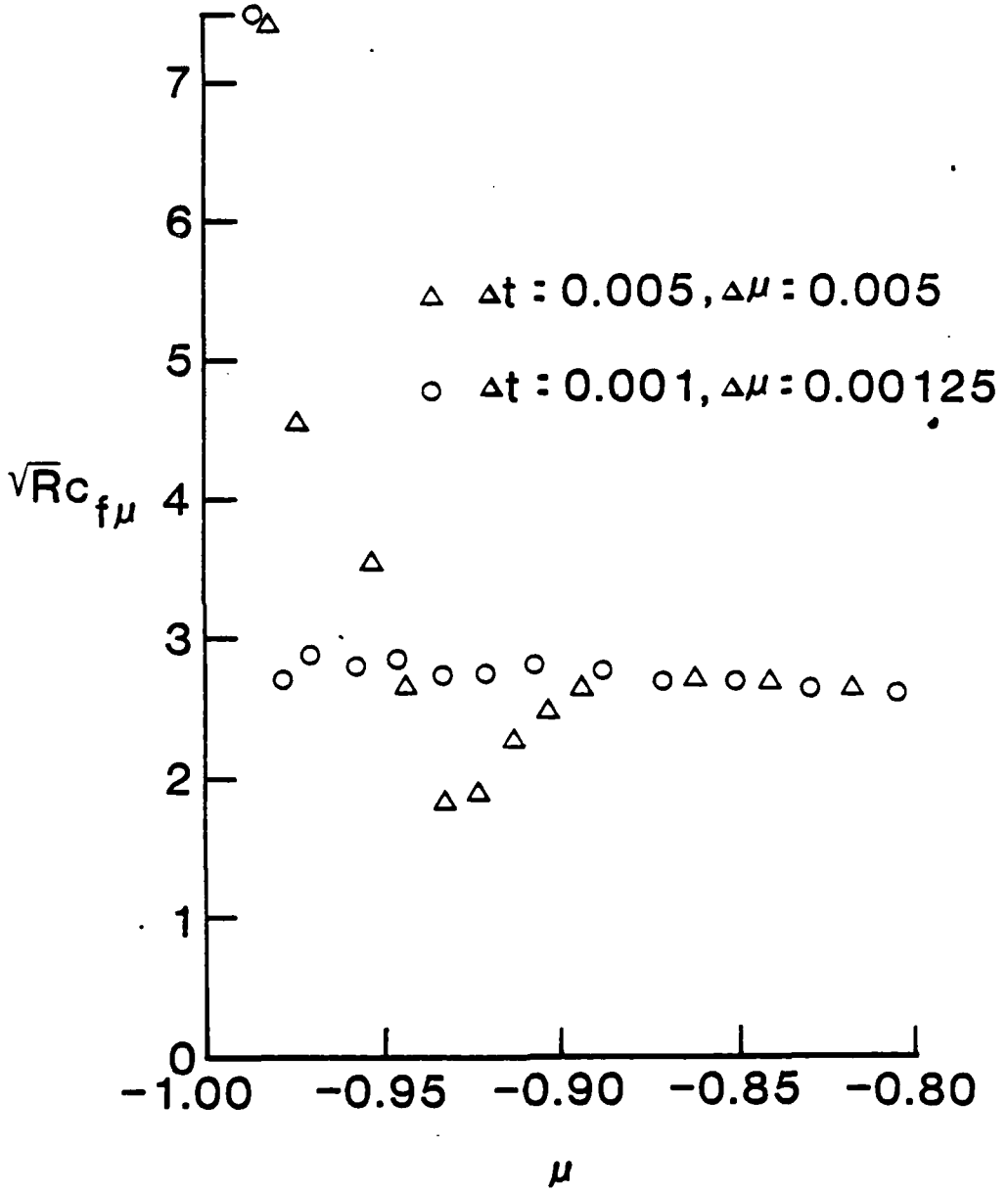

Figure 3. Comparison of different meshes

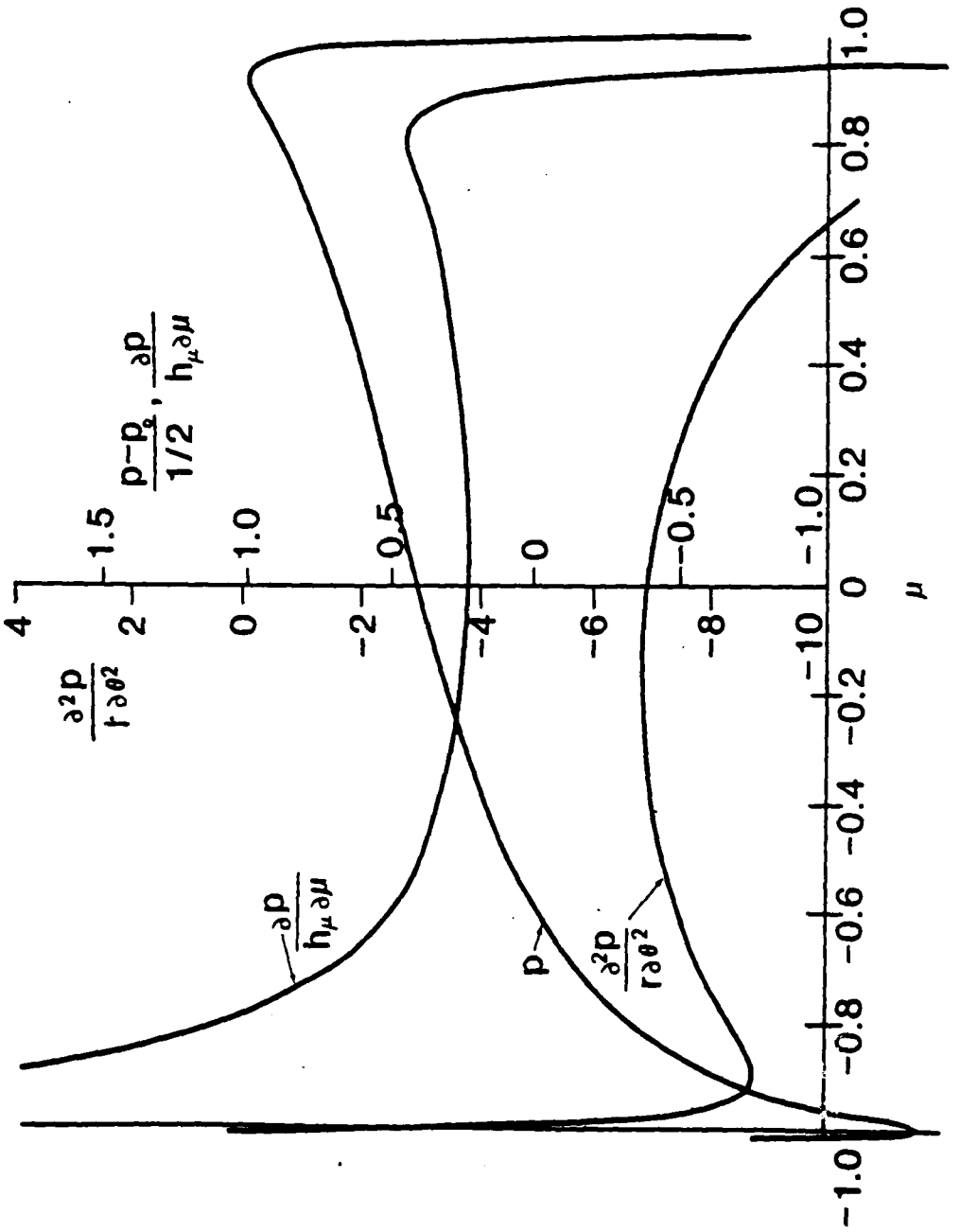

Figure 4. Pressure, pressure gradient and pressure curvature

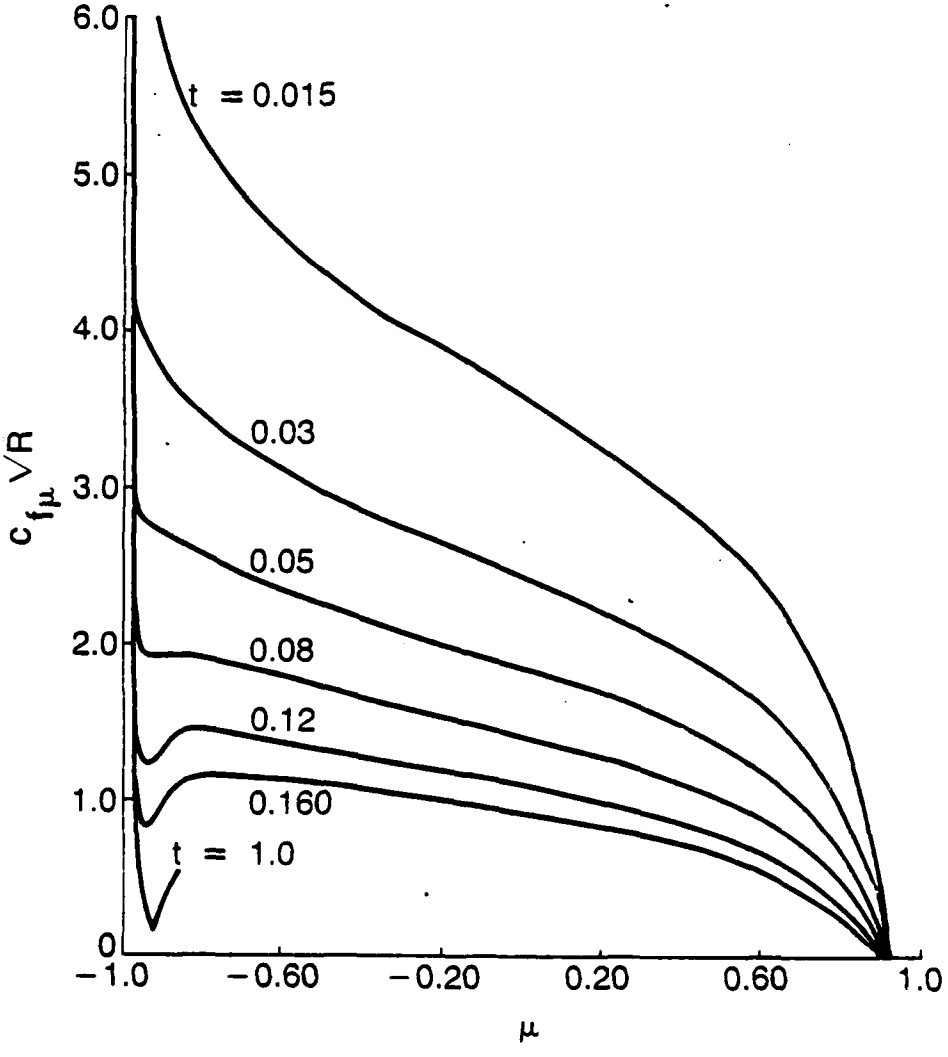

Figure 5(a). Variation of the meridional skin friction $c_{f\mu}$

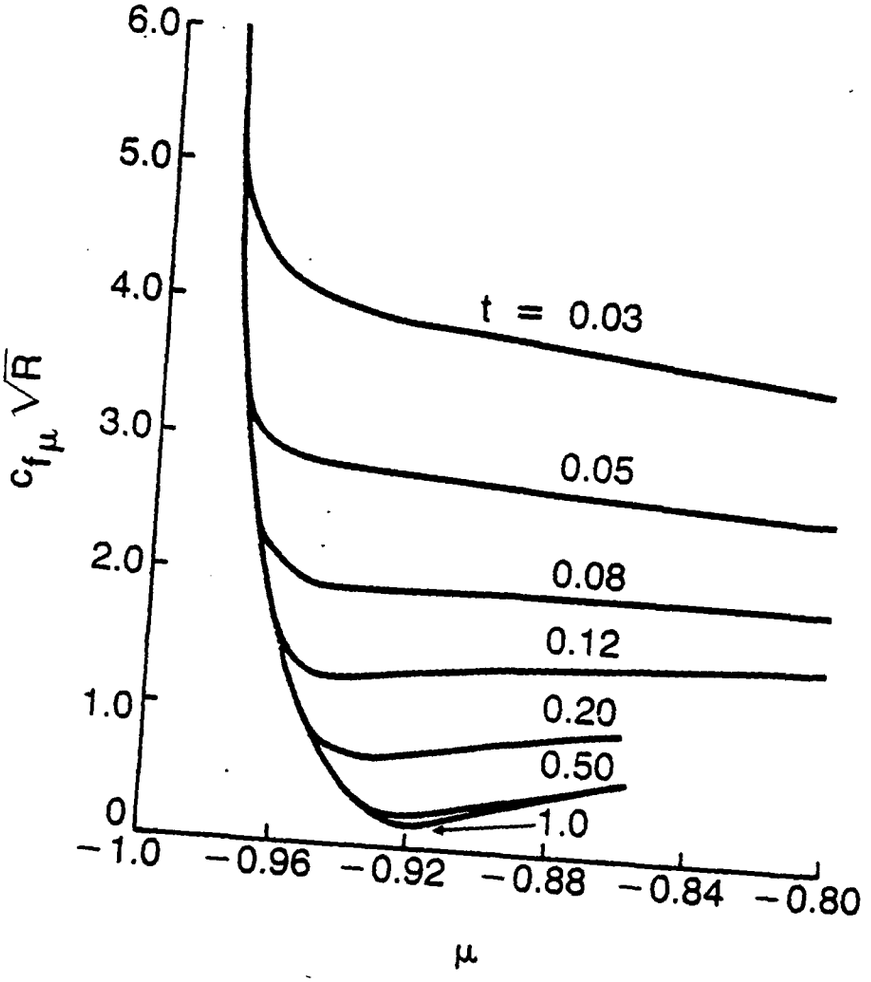

Figure 5(b). $c_{f\mu}$ near the front end

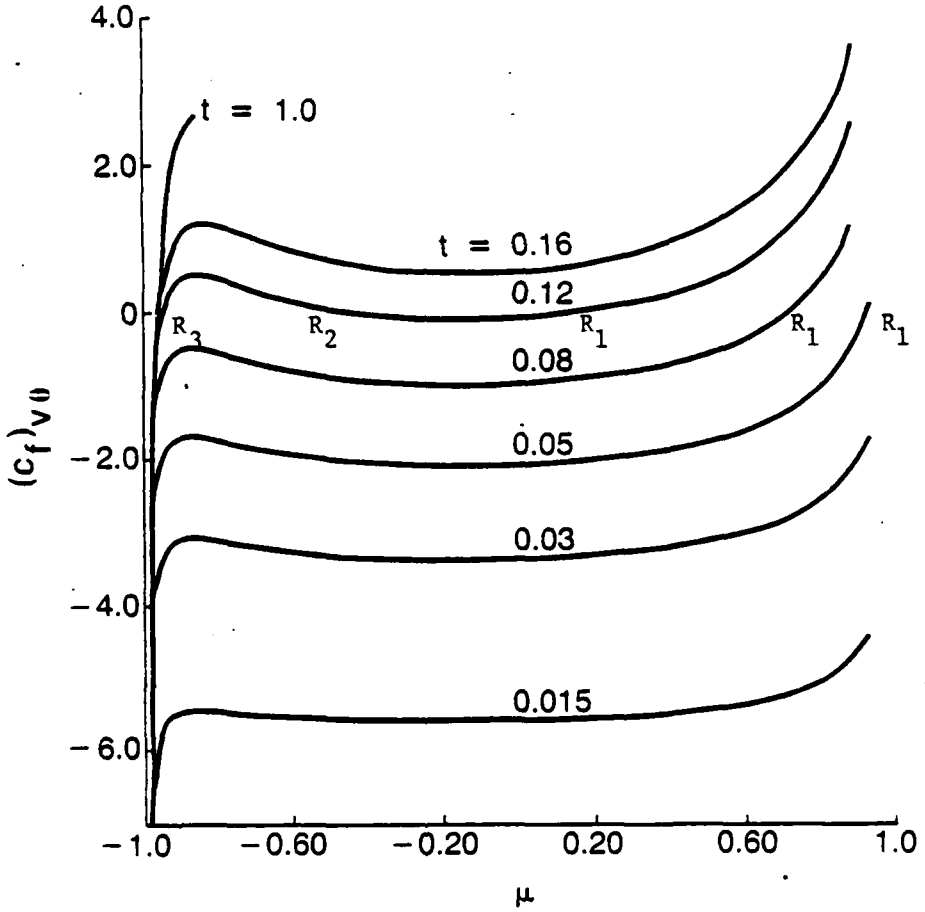

Figure 6(a) Variation of $(c_f)_{v\theta}$

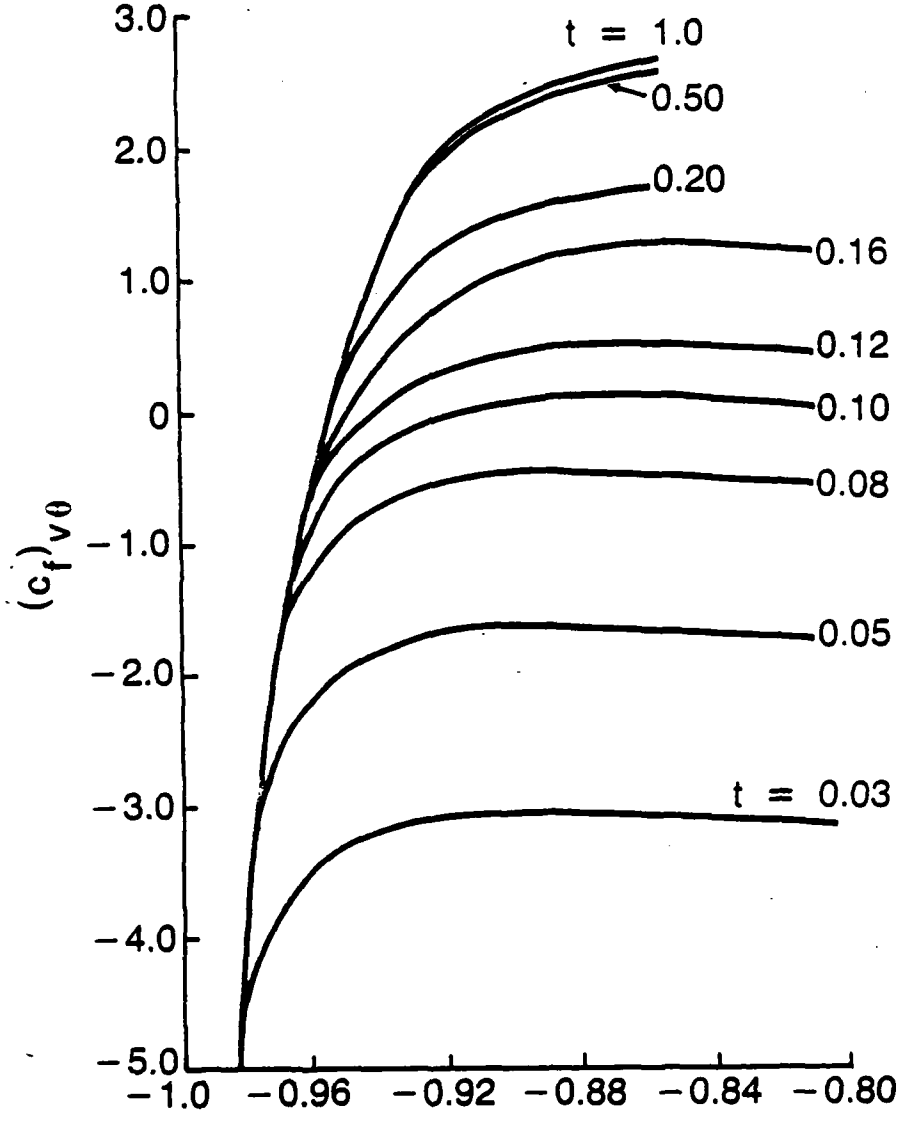

Figure 6(b). $(C_f)_{v\theta}$ Near the front end

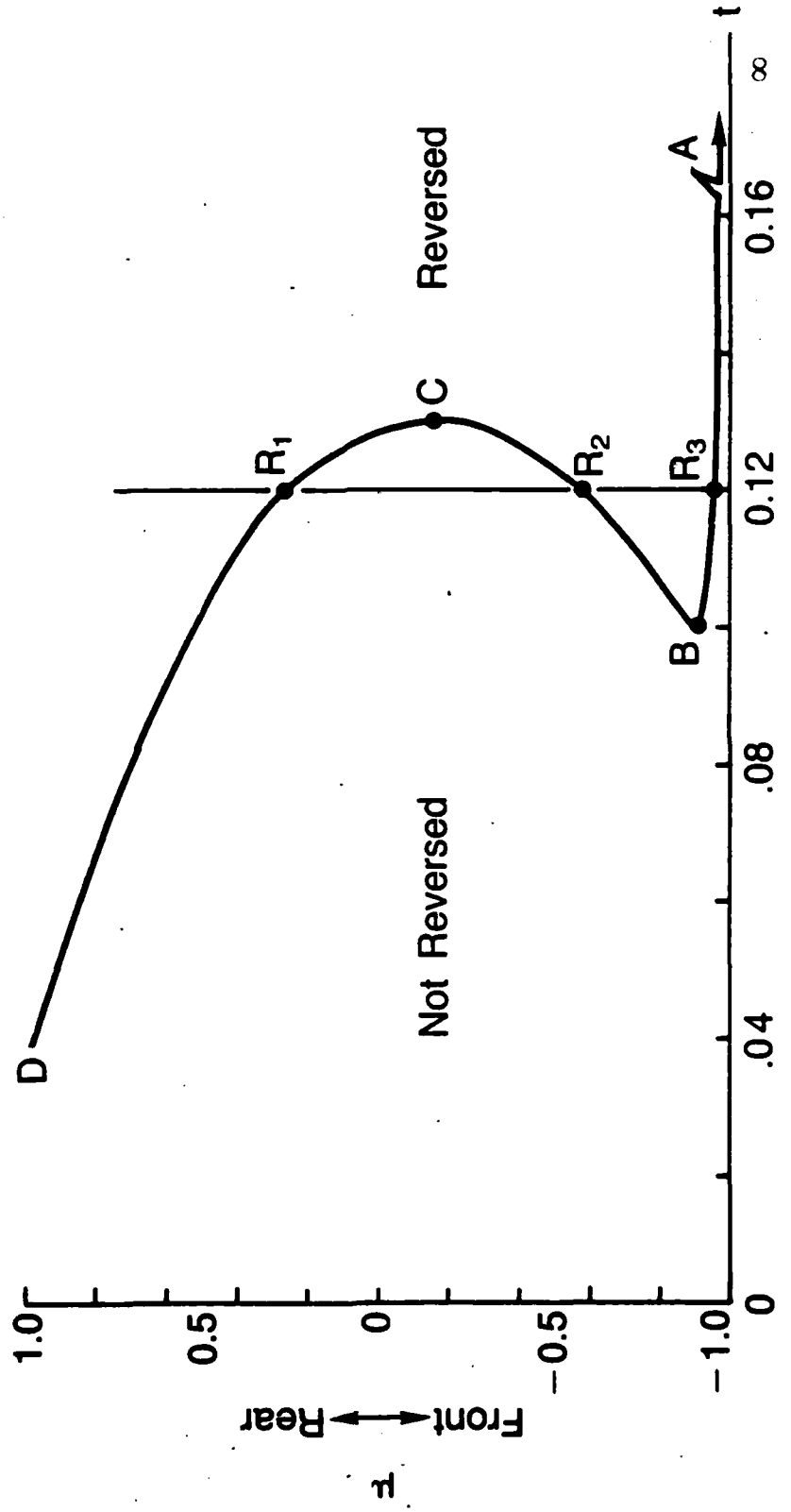

Figure 6(c). Movement of the zero-$(C_f)_{v\theta}$ point(s)

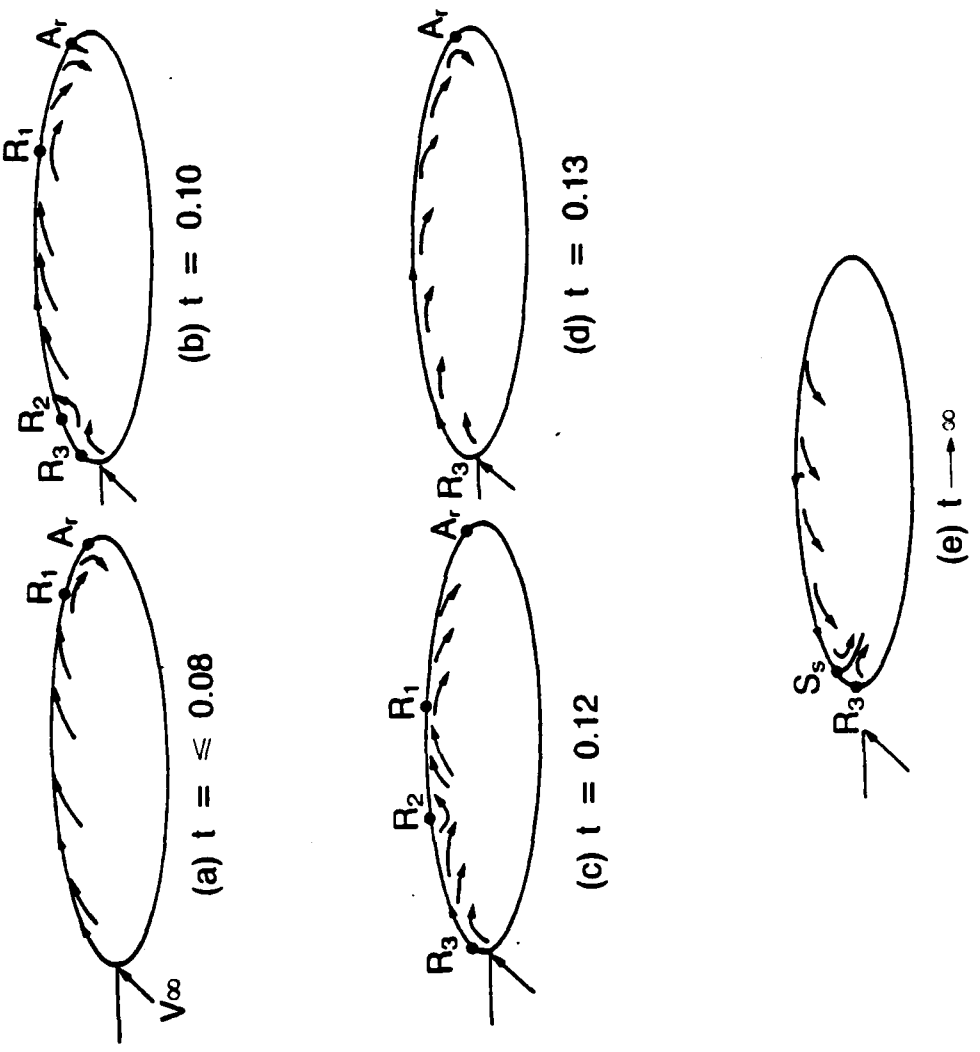

Figure 7. Flow patterns near the symmetry-plane

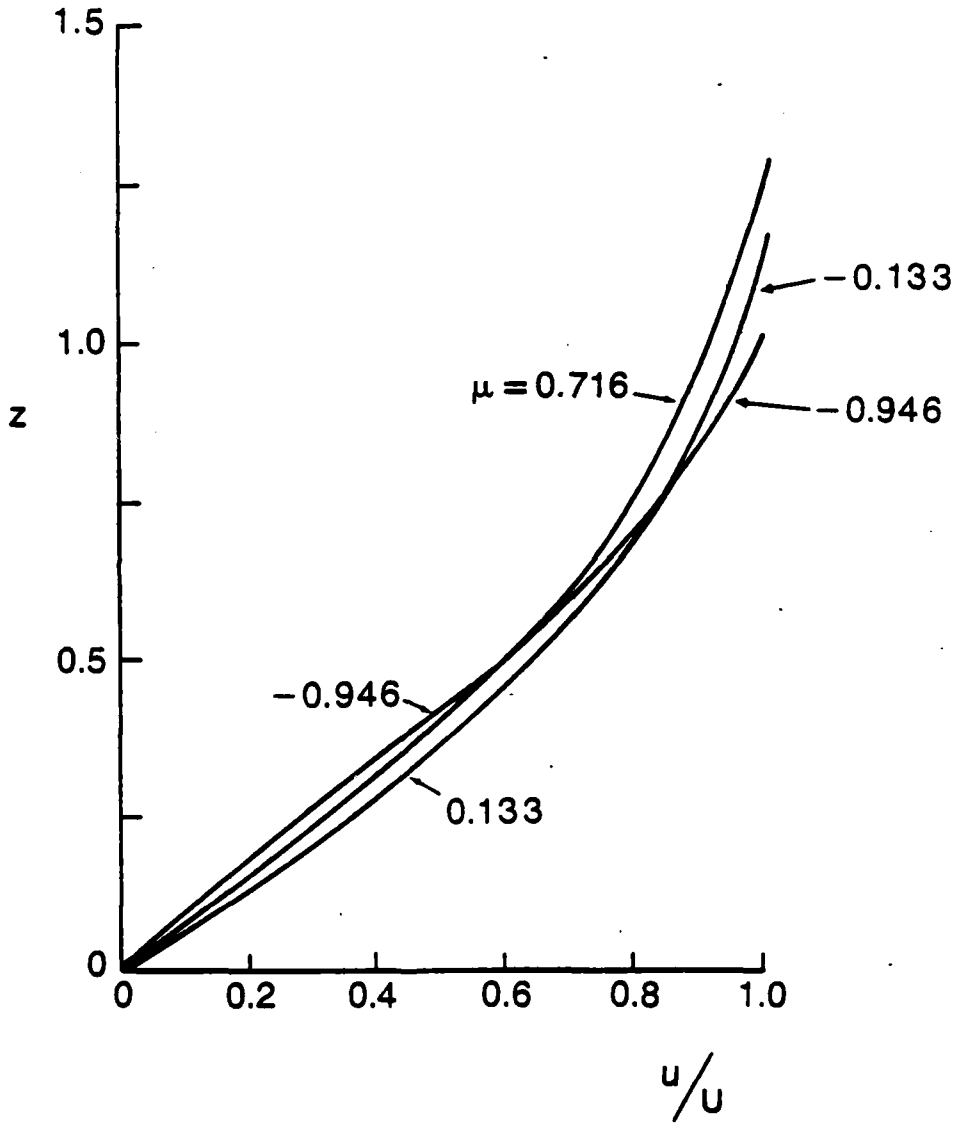

Figure 8(a). u-velocity profiles at t = 0.12

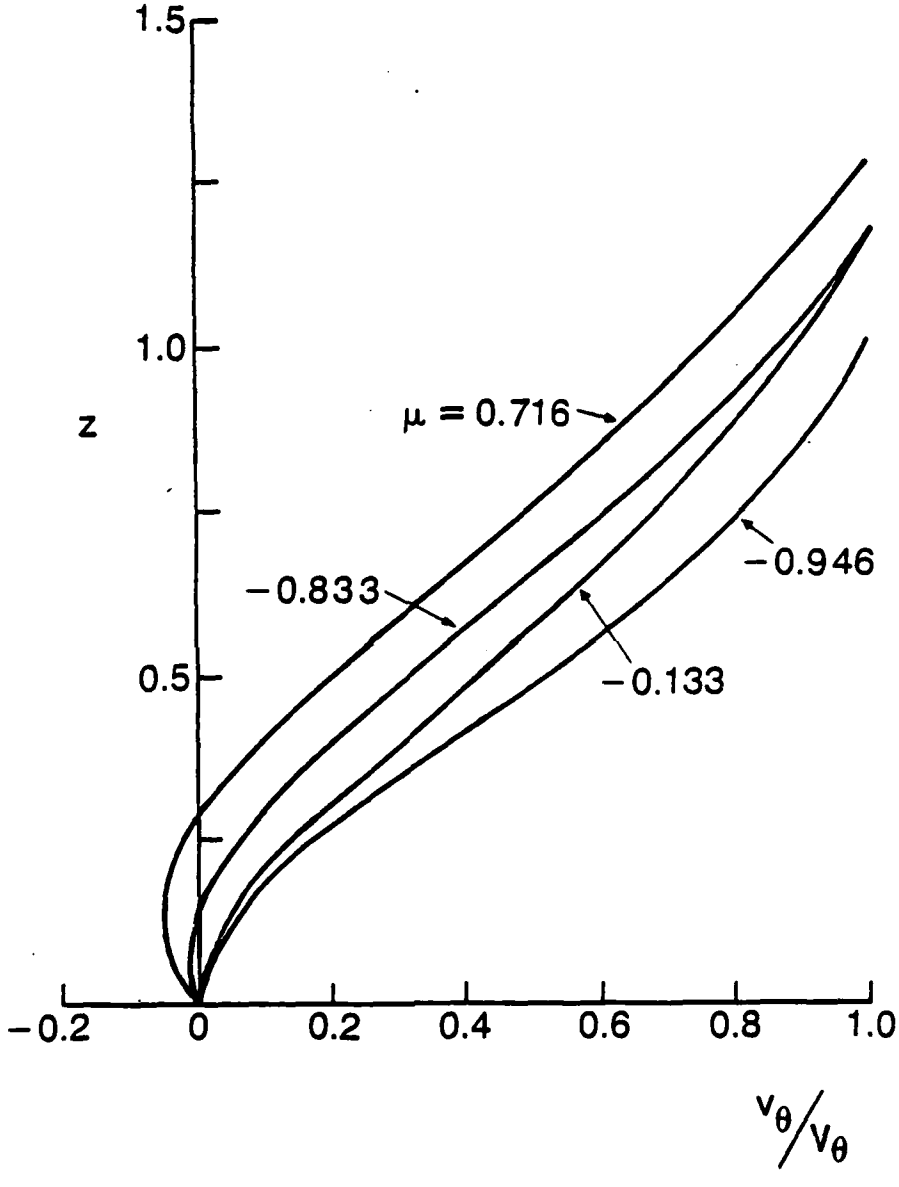

Figure 8(b). Profiles of v_θ/V_θ at t = 0.12

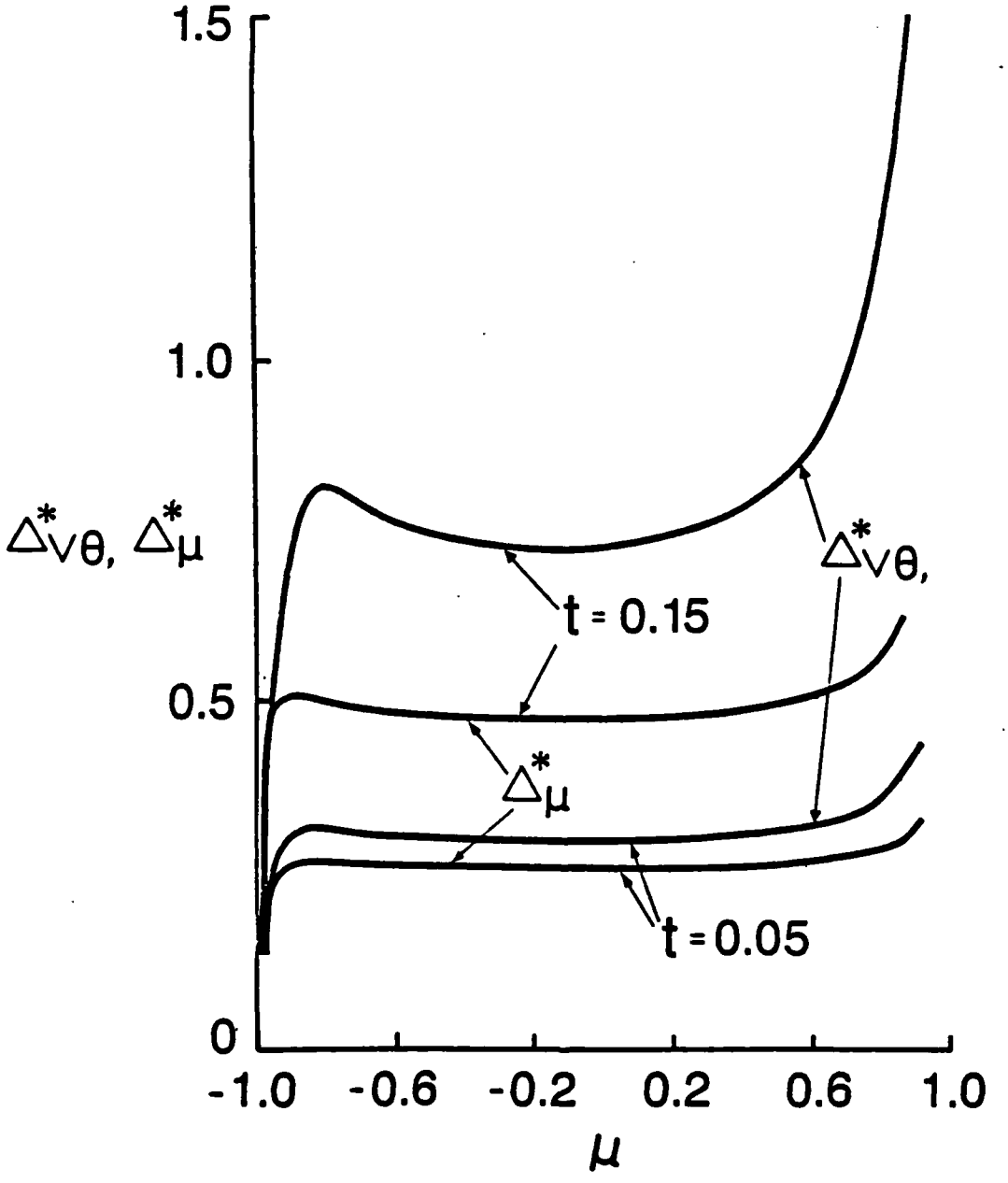

Figure 9. Displacement Thicknesses, Δ^*_{μ} and $\Delta^*_{v\theta}$

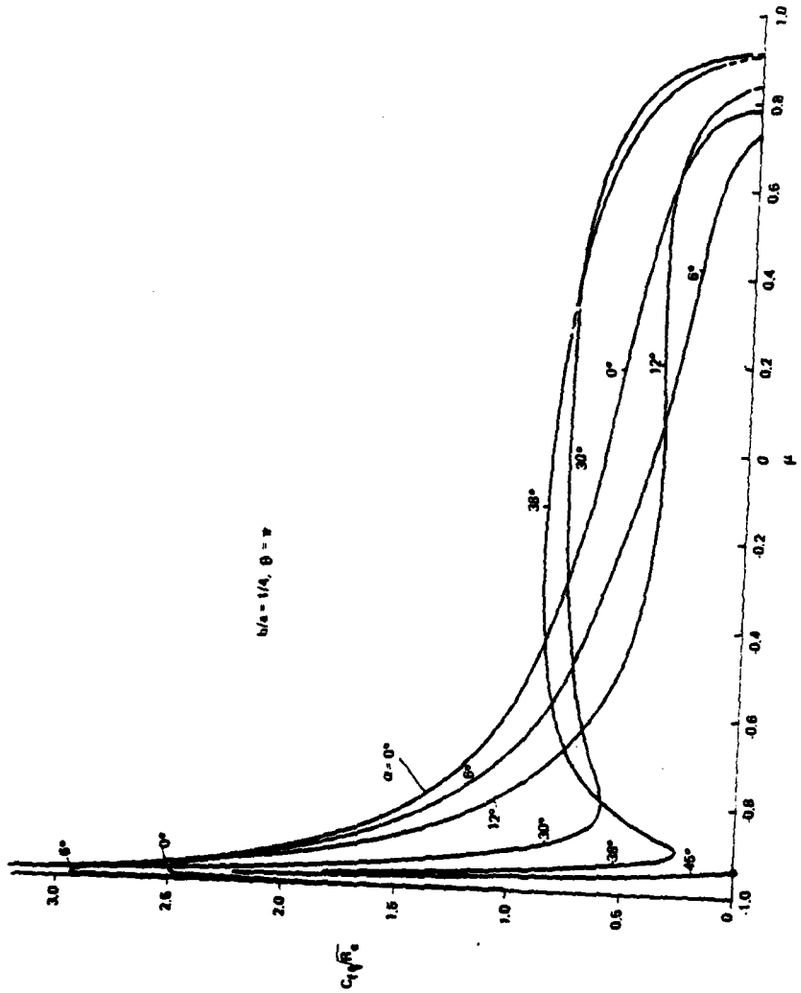

Figure 10 . Steady-flow skin friction on the leeside symmetry-plane

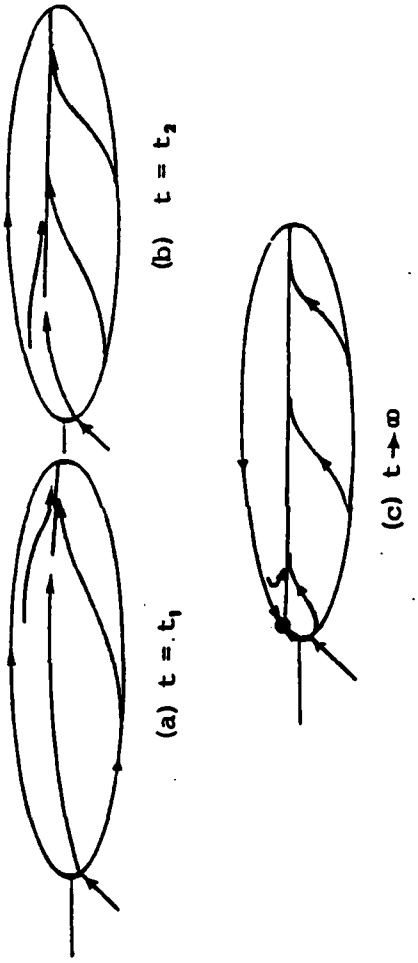

Figure 11. Proposed sequence of unsteady separation

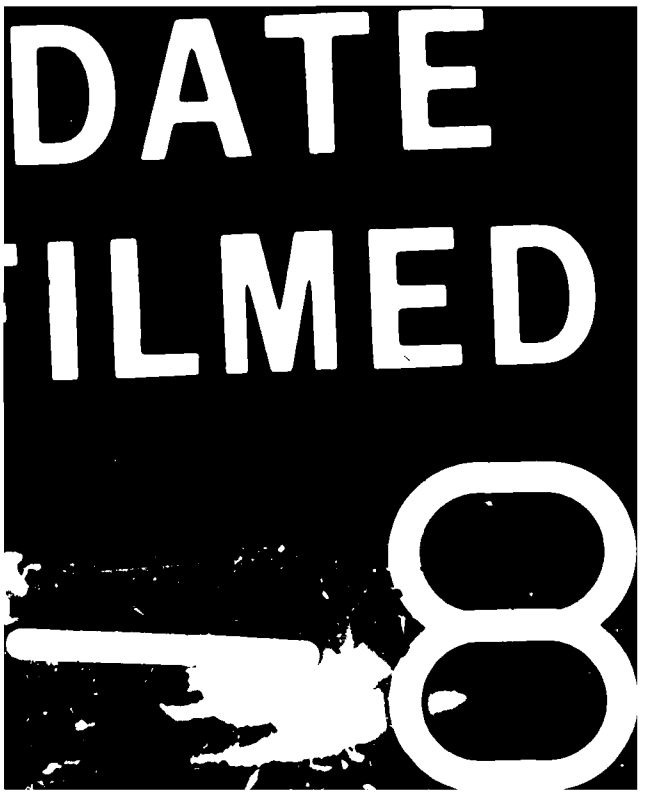
DATE
ILMED
8